Lattice dynamics and inelastic neutron and synchrotron scattering cross-sections in Nd_2CuO_4

1994 J. Phys.: Condens. Matter 6 3669

(http://iopscience.iop.org/0953-8984/6/20/007)

J. Phys.: Condens. Matter 6 (1994) 3669–3678. Printed in the UK

Lattice dynamics and inelastic neutron and synchrotron scattering cross-sections in Nd_2CuO_4

M Hofmann, D Strauch, U Schröder and E Rampf
Institut für Theoretische Physik, Universität, D-93040 Regensburg, Germany

Received 14 December 1993, in final form 7 February 1994

Abstract. Different shell models for Nd_2CuO_4 reproduce the phonon dispersion curves comparably well. Even though the phonon frequencies are practically the same in the different models the phonon eigenvectors and thus the phonon spectra depend very sensitively on the shell model parameters. In this paper we compare theoretical neutron and synchrotron one-phonon scattering cross-sections.

1. Introduction

Inelastic scattering experiments give information about elementary excitations in solids. Particularly neutron scattering is a useful method of determining lattice-dynamical properties. In recent years the use of synchrotron sources for the experimental determination of the phonon dispersion has also been proved successful [1] . This is the only method if the crystal size is too small for neutron scattering experiments unless many samples are aligned on the same sample holder [2]. In this case the use of synchrotron scattering is preferred over the use of neutron scattering because a larger flux can be obtained, and the cross-section for atoms with a high atomic number is larger. Thus, the first aim of the present work is a comparative study of the one-phonon cross-sections for the scattering of thermal neutrons and of synchrotron radiation.

The second object of the present work is to stress that scattering spectra contain more information than just about the phonon frequencies. Lacking *ab initio* results for more complicated substances lattice-dynamical models must be employed. The model, whose parameters are fitted to the experimentally determined frequencies at a selected set of high-symmetry wavevectors, is designed to interpolate for the experimentally unknown frequencies in other directions.

However, the knowledge of only the eigenvalues ω^2 does not uniquely determine the force constants [3] because a unitary transformation of the eigenvectors $\boldsymbol{u}$

$$\mathbf{D}\boldsymbol{u} = \omega^2\boldsymbol{u} \quad \Leftrightarrow \quad \mathbf{U}\mathbf{D}\mathbf{U}^{-1}\mathbf{U}\boldsymbol{u} = \omega^2\mathbf{U}\boldsymbol{u}$$

is also a solution of the eigenvalue problem with the same eigenvalue; here $\mathbf{U}$ is an arbitrary unitary matrix, and $\mathbf{D}$ is the dynamical matrix which contains the force constants. Thus, we secondly compare scattering spectra which are obtained from different lattice-dynamical shell models with practically the same phonon frequencies but different eigenvectors.

We have selected Nd_2CuO_4 as the object of our investigations because of the present general interest in high-temperature superconductors on the one hand and because of its relatively simple structure on the other, with just three atom types per elementary cell [4]; finally, these samples are usually of a small size for which synchrotron scattering is the only feasible method.

0953-8984/94/203669+10$19.50

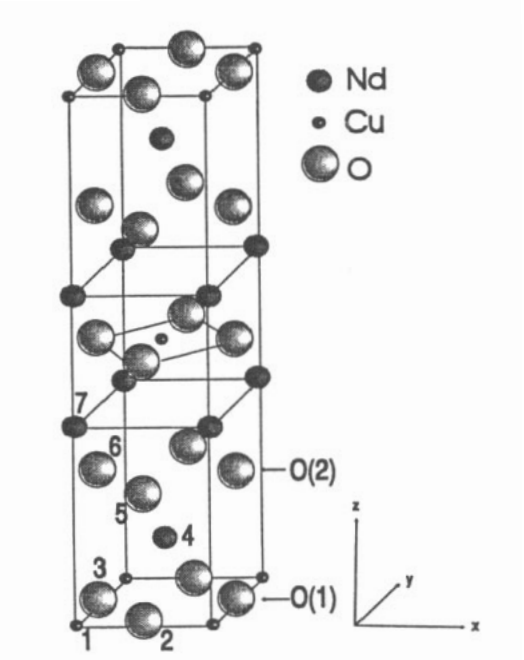

Figure 1. Body-centred tetragonal elementary cell of Nd_2CuO_4 (contains two primitive unit cells).

Table 1. Short-range longitudinal (L) and transverse (T) force constants (in units of N m^{-1}) of models A and B. (Model A is identical to model II of [9].)

	L		T	
Bond/Model	A	B	A	B
1 Cu – 2 O(1)	273.1	294.7	−36.8	−36.8
1 Cu – 5 O(2)	0.5	0.1	0.0	0.0
4 Nd – 2 O(1)	102.3	100.7	−12.1	−12.1
4 Nd – 5 O(2)	231.3	230.2	−29.8	−29.8
2 O(1) – 3 O(1)	−3.6	20.0	0.5	0.5
2 O(1) – 5 O(2)	−1.8	−1.1	0.3	0.3
5 O(2) – 6 O(2)	−3.6	18.8	0.5	0.5

Table 2. Shell charges Y and ion charges Z (in units of the elementary charge e), and polarizabilities α (in units of $Å^3$) for Nd_2CuO_4.

	Y		Z		α_x		α_y		α_z	
Ion/Model	A	B	A	B	A	B	A	B	A	B
1 Cu	2.8	3.4	1.9	1.9	0.980	0.734	0.980	0.734	0.980	0.743
2 O(1)	−2.7	−2.1	−1.9	−1.9	0.420	2.558	0.420	3.635	2.800	3.453
4 Nd	1.3	0.7	2.6	2.6	1.346	3.341	1.346	3.341	1.346	0.501
5 O(2)	−2.7	−3.2	−1.65	−1.65	1.870	0.691	1.870	0.691	1.050	1.061

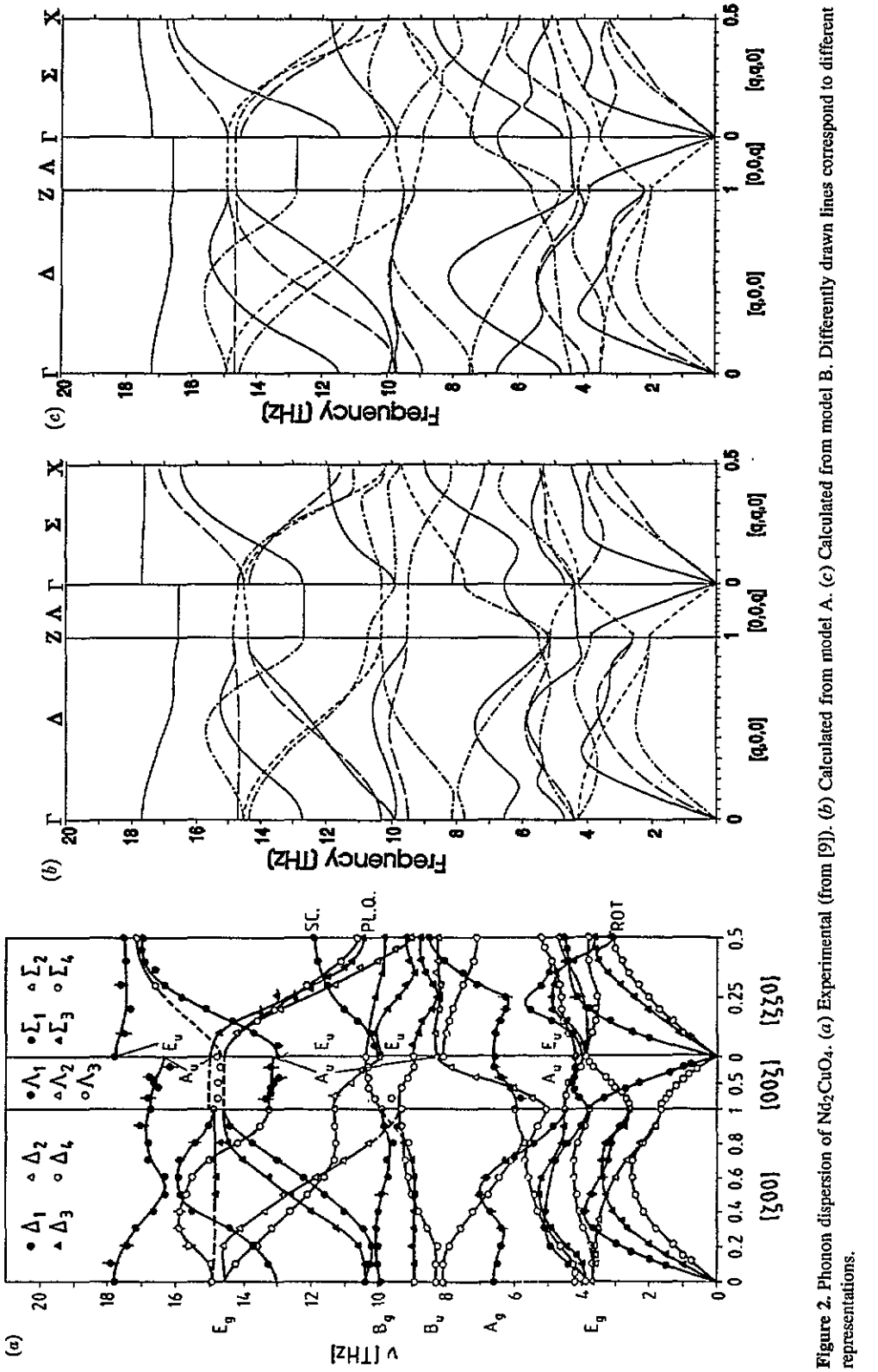

Figure 2. Phonon dispersion of Nd_2CuO_4. (*a*) Experimental (from [9]). (*b*) Calculated from model A. (*c*) Calculated from model B. Differently drawn lines correspond to different representations.

2. Lattice-dynamical shell models for Nd_2CuO_4

Nd_2CuO_4 is one of the high-temperature superconducters with a simple structure. It is a perovskite-type body-centred tetragonal T' structure with seven particles per unit cell (see figure 1) and with an I4/mmm point group [5]. In the undoped case Nd_2CuO_4 behaves like an antiferromagnetic insulator with a Néel temperature of $T_N = 245$ K [6]. Doping with Ce leads to metallic behaviour of the CuO_2 planes, and $Nd_{2-x}Ce_xCuO_4$ becomes an *n*-type superconductor at the critical temperature of $T_c = 23$ K if $x \simeq 0.15$ [7, 8].

The mostly ionic character of the pure crystal with polarizable ions is accounted for by lattice-dynamical shell models [9]. We have used two different models. In the first model (model A, identical to model II of [4]) we have assumed the polarizibility only for the oxygen ions to be anisotropic. In the second model (model B) we have additionally included the anisotropy of the polarizibility for the Nd ions to account for the anisotropic coordination of these ions. The short-range force constants are listed in table I; charges and polarizabilities are listed in table II. The charges and the transverse force constants, if assumed to be derivable from a central potential, fulfill the equilibrium conditions.

Compared with the experimental phonon dispersion curves obtained by Pintschovius *et al* [10] (see figure 2(*a*)) both shell models describe the neutron-scattering data qualitatively well. The differences between model A (figure 2(*b*)) and model B (figure 2 (*c*)) are small: in comparison with the experimental results model A describes the low-lying Δ-branches better than model B, but the upper Δ-branches are better described by model B. The anti-crossing effect between the two lowest optical modes is better described by model A.

3. Synchrotron- and neutron-scattering intensities

The measured scattering intensity $I(Q_0, \omega_0)$ for momentum transfer $\hbar Q = \hbar(G + q)$ and energy transfer $\hbar\omega_0$ is given by the convolution

$$I(Q_0, \omega_0) = \int S(Q, \omega) R(Q - Q_0, \omega - \omega_0)\, \mathrm{d}^3Q\, \mathrm{d}\omega \tag{1}$$

where $R(Q, \omega)$ is the instrumental resolution function and $S(Q, \omega)$ is the scattering law. While the resolution function is particular to the instrument, the scattering law is given by the phonon structure of the material under investigation.

The cross-section for coherent scattering is related to the scattering law by [11]

$$\frac{\mathrm{d}^2\sigma}{\mathrm{d}\omega\, \mathrm{d}\Omega} = C^2 \frac{k_f}{k_i} S(Q, \omega)$$

with the scattering function (for harmonic phonons)

$$S(Q, \omega) = \frac{N\hbar}{2} \sum_{qj} \sum_{G} F(Q)\, \delta_{Q, q+G} \frac{1}{\omega_j(q)} \big[(n_j(q) + 1)\, \delta(\omega_j(q) - \omega) + n_j(q)\, \delta(\omega_j(q) + \omega)\big]$$

$$= N \frac{\hbar}{2} \frac{1 + n_\omega}{\omega} \sum_{qj} \sum_{G} F(Q)\, \delta_{Q, q+G} \big[\delta(\omega_j(q) - \omega) + \delta(\omega_j(q) + \omega)\big]$$

and the Bose factor

$$n_\omega = \frac{1}{e^{\beta\hbar\omega} - 1} = -1 - n_{-\omega}\,.$$

$F(Q)$ is the dynamical structure factor, $k_i = k_f + Q$ and k_f are the wavevectors of the incoming and scattered radiation. This equation applies to synchrotron as well as to neutron scattering.

For *synchrotron* scattering one has [1]

$$C = \frac{e^2}{m_e c^2}(\epsilon_{k_i\sigma_i} \cdot \epsilon_{k_f\sigma_f})$$

and

$$F(Q) = \left| \sum_\kappa f_\kappa(Q) \exp\{-W_\kappa(Q)\}\, Q \cdot u(\kappa|q, j) \exp\{-iG \cdot R(\kappa)\} \right|^2 .$$

$u(\kappa|q, j)\sqrt{M_\kappa}$ is the phonon polarization unit vector of a phonon with branch index j and wavenumber q of the atom at the basis vector $R(\kappa)$ within the unit cell. e^{-W_κ} is the Debye–Waller factor, M_κ the mass and $f_\kappa(Q)$ the atomic form factor of that atom. $\epsilon_{k_f\sigma_f}$ and $\epsilon_{k_i\sigma_i}$ are the polarization vectors of the scattered and incident beam, respectively.

For *neutron* scattering one has $C = 1$, and one must replace the atomic form factor $f_\kappa(Q)$ by the Fermi scattering length b_κ, which is independent of Q.

For an easier comparison we neglect the factor $(1 + n_\omega)/\omega$ in the scattering function $S(Q, \omega)$. We thus investigate the reduced intensity (neglecting the Debye–Waller factor)

$$\tilde{F}(Q) = \left| \sum_\kappa c_\kappa(Q)\, Q \cdot u(\kappa|q, j) \exp\{-iG \cdot R(\kappa)\} \right|^2 \tag{2}$$

with

$$c_\kappa(Q) = \begin{cases} f_\kappa(Q) & \text{for synchrotron scattering} \\ b_\kappa & \text{for neutron scattering.} \end{cases}$$

In the following we will concentrate on the modes of Δ_1 and Σ_1 symmetry in Nd_2CuO_4. If one chooses the momentum transfer $\hbar Q = \hbar(q + G)$ parallel to the phonon wavenumber q and both in the [100] or [110] directions then phonons of these representations are the only ones which contribute to the scattering cross-sections. In figure 3 we show the results for equation (2) using model A. For the resolution function like in (1) we have assumed a two-dimensional Lorentzian of widths $\delta\nu = 0.055$ THz and $\delta Q = 8.3 \cdot 10^{-4}(2\pi/a)$. At the top of the figures we have given a logarithmic contour plot. Figures 3(*a*) and (*b*) show the results for neutron scattering and figures 3(*c*) and (*d*) for synchrotron scattering. The momentum transfer $\hbar Q$ is in the [100] direction for figures 3(*a*) and (*c*) and in the [110] direction for figures 3(*b*) and (*d*). The high-frequency part of the synchrotron spectra has very low intensity (figures 3(*c*) and (*d*)): at higher frequencies it is mainly the oxygen ions which are vibrating, and the atomic form factors of these ions are small compared with those of Nd and Cu. On the other hand, since the Fermi scattering length b_O is comparable to b_{Nd} and b_{Cu} the higher-frequency portions of the neutron spectra gain intensity (figures 3(*a*) and (*b*)). Also, the near equality of the Fermi scattering lengths b_{Nd} and b_{Cu} causes the neutron intensities in the [110] direction to show an asymmetric behaviour which is based on the near extinction of the scattered components for odd components of the vector G (in units of $2\pi/a$). (For even components the intensity of the acoustic modes is large, but it nearly vanishes for odd components.)

To show the physical significance of the phonon eigenvectors we have calculated the synchrotron scattering intensities for Δ_1 modes with the momentum transfer $\hbar Q$ in the

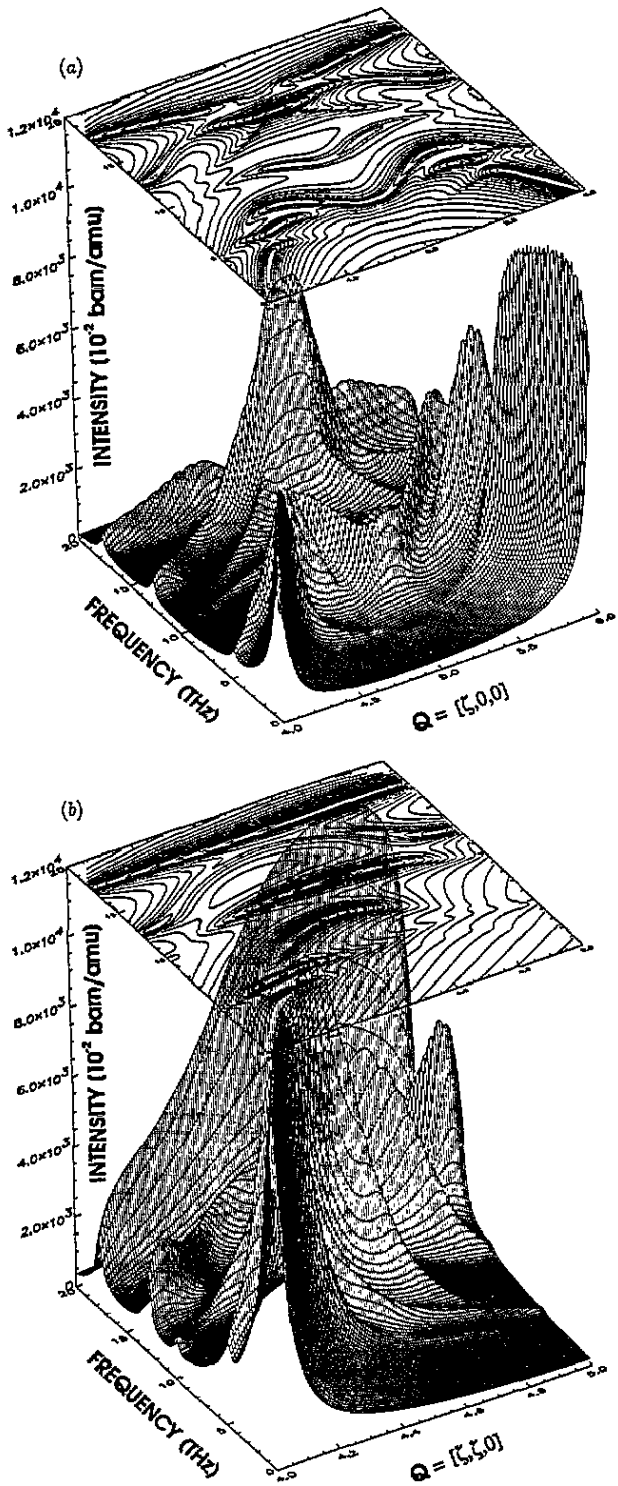

Figure 3. 3D plot and logarithmic contour plot of the reduced inelastic scattering intensity $\tilde{F}$, (2), in energy–momentum space. (*a*) and (*b*) neutron scattering; (*c*) and (*d*) synchrotron scattering; (*a*) and (*c*) [100] direction; (*b*) and (*d*) [110] direction.

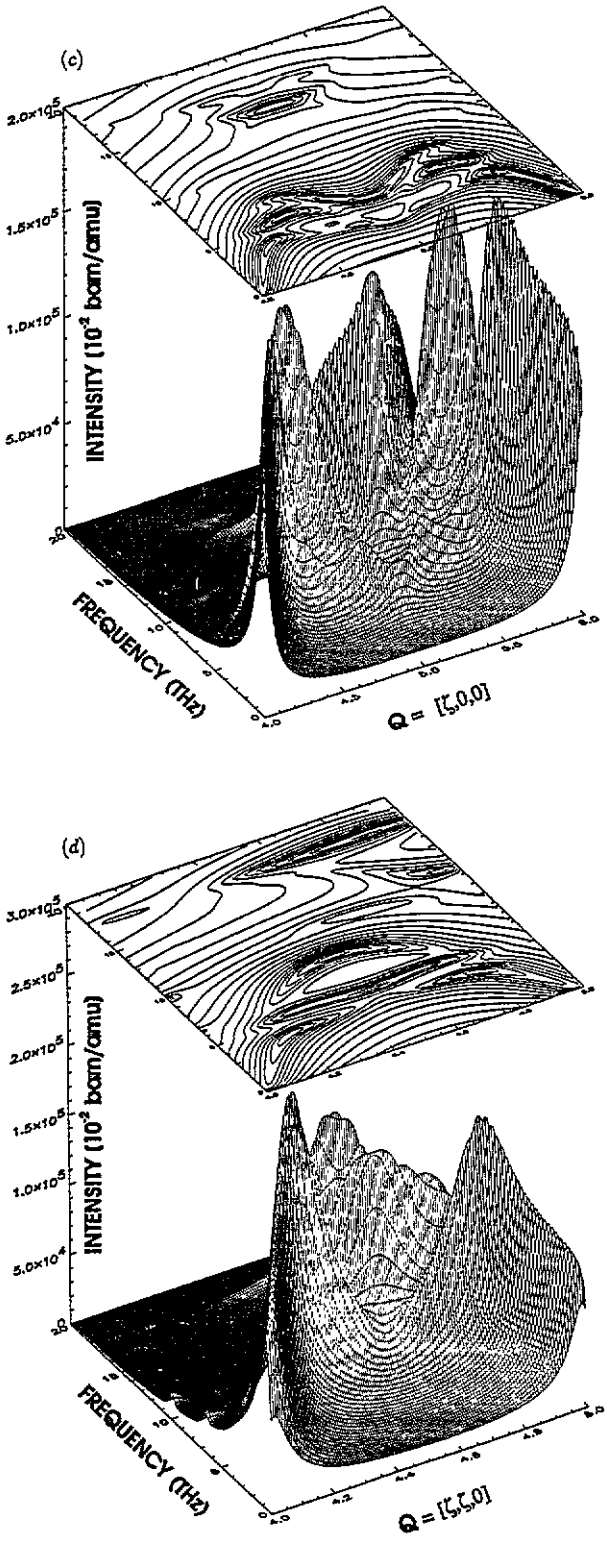

Figure 3. Continued.

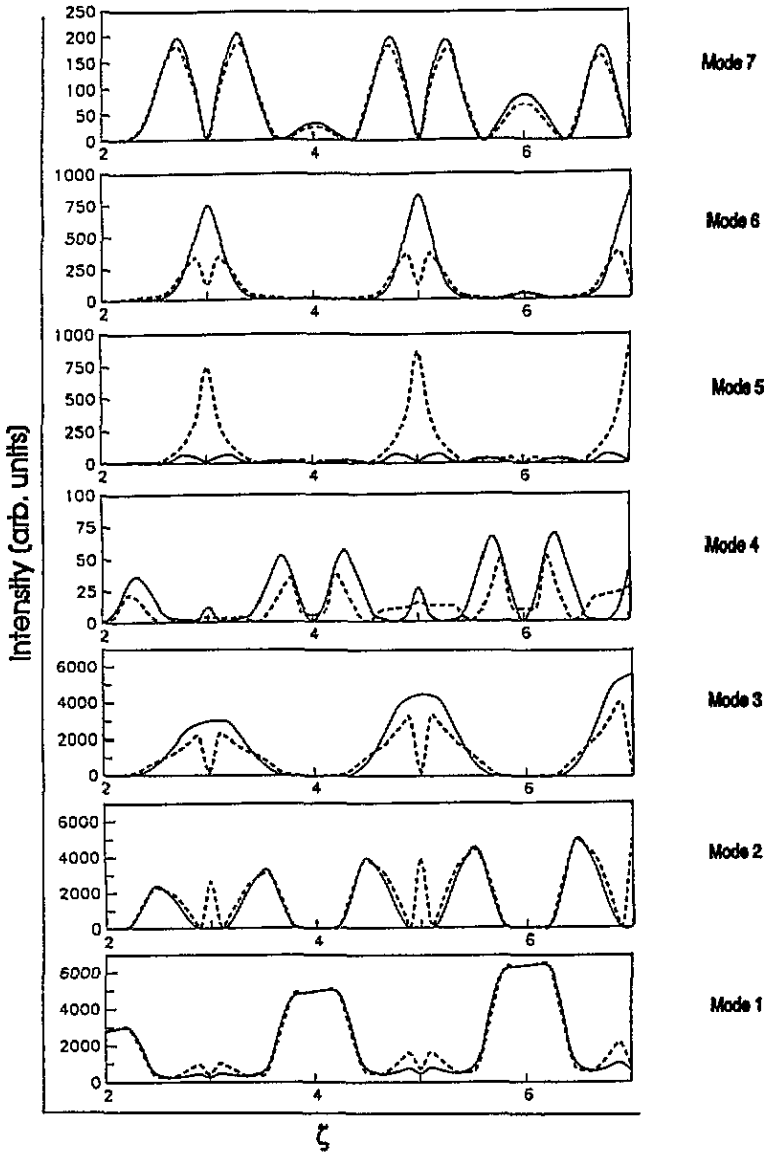

Figure 4. Theoretical reduced synchrotron scattering intensities by Δ_1 modes in Nd_2CuO_4 after model A (full lines) and model B (broken lines) for $Q = (\zeta, 0, 0)\pi/a$. The spectra for different modes are not to scale.

[1,0,0] direction based on the models A and B. In figure 4 we compare the results of our calculations for both models. The mode number on the right-hand side of figure 4 counts the Δ_1 branches from the bottom (acoustic) to the top (highest optical branch) (see figures 2(*b*) and (*c*)). We find a qualitatively and quantitatively different behaviour for the synchrotron intensities which is caused by the different eigenvectors (the eigenfrequencies are nearly the same). At the Z point of the BZ ($\xi = 3, 5, 7$ in figure 9) the two models predict drastic differences between the calculated synchrotron intensities: Where model A predicts a vanishing intensity model B predicts a maximum.

Also we find an 'exchange' of the intensities between the different branches caused

by the acoustic/optic character change of the eigenvectors u. The intensity of the first (acoustic) mode ($\xi = 2, 4, 6$) has a maximum at the Γ point (figure 4). The intensity decreases towards the middle of the BZ, and it nearly vanishes at the BZ boundary. On the other hand, the intensity of the second (lowest optical) mode becomes large where the intensity of the first mode disappeares, i.e. where the eigenvectors u acquire an acoustic character.

4. Summary and conclusions

We have studied the synchrotron- and neutron-scattering intensities for the high-temperature superconductor Nd_2CuO_4 based on shell-model calculations. We have demonstrated that scattering intensities strongly depend upon the model force constants and thus phonon eigenvectors, although the eigenfrequencies are nearly the same.

The higher phonon frequencies are generally caused by the lighter atoms, and since the atomic form factors are smaller the lighter the atoms are, the higher-frequency portions of the synchrotron spectra are weak. This is also the case for Nd_2CuO_4 where the higher frequencies are caused mainly by the oxygen atoms with the atomic form factor f_O being small compared with f_{Nd} and f_{Cu}.

In contrast to the synchrotron spectra, the high-frequency vibrations do contribute to the neutron spectra since the scattering lengths b_κ for the constituents of Nd_2CuO_4 are nearly the same. The near equality in particular of b_{Nd} and b_{Cu} also leads to the asymmetric behaviour of the neutron intensities in the [110] direction whereas the synchrotron intensities behave symmetrically. Anyway, in both inelastic scattering techniques the high-frequency modes have lower intensity due to the factor $1/\omega$ in the scattering cross-section which was neglected in the calculation of the reduced intensity $\tilde{F}$. Thus, in addition to the information about the phonon frequencies, the intensity distribution of spectra contains information about the phonon eigenvectors, and the more detailed analysis of the latter is essential to discriminate between the various models and ultimately to determine the interionic interaction strengths.

Synchrotron and neutron experiments are complementary, and experiments with the former technique are overdue.

Acknowledgments

This work was supproted in part by the Bundesministerium für Bildung und Wissenschaft, the Bundesministerium für Forschung und Technologie and by the Deutsche Forschungsgemeinschaft (Graduiertenkolleg Komplexität).

References

[1] Burkel E 1991 *Inelastic Scattering of X-Rays with Very High Energy Resolution, Springer Tracts in Modern Physics* vol 125 (Berlin: Springer)
[2] Pintschovius L 1990 *Festkörperprobleme* vol 30, ed U Rößler (Braunschweig: Vieweg) p 183
[3] Leigh R S, Szigeti B and Tewary V K 1971 *Proc. R. Soc.* A **320** 505
[4] Rampf E, Schröder U, de Wette F W, Kulkarni A D and Kress W 1993 *Phys. Rev.* B **48** 10 143
[5] Müller-Buschbaum H and Wollenschläger W 1980 *Z. Anorg. Allg. Chem.* **414** 76
[6] Heyen E T, Kliche G, Kress W, König W, Cardona M, Rampf E, Prade J, Schröder U, Kulkarni A D, de Wette F W, Piñol S, Paul D McK, Morán E and Alario-Franco M A 1990 *Solid State Commun.* **74** 1299
[7] Tokura Y, Takagi H and Uchida S 1989 *Nature* **337** 345

[8] Takagi H, Uchida S, Tokura Y 1989 *Phys. Rev. Lett.* **62** 1197
[9] Woods A D B, Cochran W, Brockhouse B N 1960 *Phys. Rev.* **119** 980
[10] Pintschovius L, Pyka N, Reichardt W, Rumiantsev A Yu, Mitrofanov N L, Ivanov A S, Collin G and Bourges P 1991 *Physica* C **185–189** 156
[11] Ludwig W 1967 *Recent Developments in Lattice Theory, Springer Tracts in Modern Physics* vol 43, ed G Höhler (Berlin: Springer)